Journal of Photochemistry & Photobiology, A: Chemistry 416 (2021) 113325

Contents lists available at ScienceDirect

Journal of Photochemistry & Photobiology, A: Chemistry

journal homepage: www.elsevier.com/locate/jphotochem

Effect of triptycene unit on the performance of porphyrin-based dye-sensitized solar cells

Mao Yan, Qun-Hui Wang, Yi-Zhou Zhu *, Ming-Liang Han, Yi-Qiao Yan, Jian-Yu Zheng *

State Key Laboratory and Institute of Elemento-Organic Chemistry, College of Chemistry, Nankai University, Tianjin, 300071, China

ARTICLE INFO

Dedicated to the 100th Anniversary of Chemistry at Nankai University.

Keywords:
Triptycene
Steric hindrance group
Charge recombination
Porphyrin
Photovoltaic performance
Dye-sensitized solar cells

ABSTRACT

Triptycene has been first introduced into porphyrin sensitizers (**JY74** and **JY75**) for dye sensitized solar cells. Compared to reference dye **YD26**, the homoaromatic electron delocalization of triptycene makes the designed dyes a broadened absorption. Meanwhile, the rigid shape-persistent character of triptycene endows **JY74** and **JY75** an improved ability to diminish the charge recombination between electrolyte and semiconductor TiO_2. As a result, after structural modification, larger short-circuit current and higher open-circuit voltage are achieved for dyes **JY74** and **JY75**. The power conversion efficiency of **JY75** is increased by 26.8 % compared to that of **YD26**. Consequently, triptycene may be a promising bulky steric hindrance group for decorating photosensitizer to get an attractive photovoltaic performance.

1. Introduction

Highly efficient and sustainable applications of renewable energy have shown increasing importance to address the worsening energy and environmental crisis. Due to its distinctive features in high power conversion efficiency (PCE), easy fabrication, and low cost, dye-sensitized solar cell (DSSC) has attracted broad attentions of worldwide scientists and engineers in the past three decades [1]. As a core component of DSSC, the design of dye molecules presents a decisive impact on the photovoltaic properties of devices. Various metal complex dyes [2], porphyrin-based dyes [3–6], metal-free organic dyes [7–9], and so on, have been created and applied in this domain [10]. And the efficient suppression of charge recombination between the electrolyte and TiO_2 has been proven to be one of the key factors for achieving an attractive device performance, it is certainly a challenging work to bring out a dye molecule with a harmonization between broad absorption and weak charge recombination. One trustworthy solution to address this scientific problem is decorating the dye skeleton with bulky blocking group at its peripheral electron donor [11,12]. The enhanced outer volume would make the dye layer on TiO_2 more crowded, resulting in a dense surface to keep the electrolytes away from the TiO_2 semiconductor. For instance, benefitted from the more diminished recombination, dye D25L6 with triphenylamine (TPA) donor containing dodecyloxy chains gives an obviously larger open-circuit voltage (V_{OC}) of 706 mV compared to D9L6 (640 mV) with methoxy modification [13]. Also, TPA donor featuring two additional bis(2,4-dialkoxy)benzene could not only improve the solubility, but also decrease charge recombination, leading to enhanced short-circuit current (J_{SC}) and V_{OC} [14]. Until now, most of the researches are focusing on the flexible steric hindrance groups, but reports based on rigid steric hindrance groups are rare [15,16].

The triptycene and its derivatives are a well-known class of rigid and shape-persistent organic frameworks, where two bridgehead carbon atoms are symmetrically attached by three aromatic rings, and any two of them take a dihedral angle at 120 degrees, sustaining a butterfly-shaped three-dimensional structure [17]. Photoelectron spectroscopic studies suggest that there is an electronic communication between the three aromatic units of triptycene through a dominant through-space interactions [18]. That might be helpful for triptycene-involved molecules to get better charge separation and transportation [19]. Owing to its unique configuration, interesting electrochemical and photochemical properties, triptycene-contained molecules have been extensively applied as potential optoelectronic materials [20,21].

As mentioned above, the butterfly-like triptycene could be used as a building block to decorate the donor of dye molecule in DSSC, and the inherent steric effect of triptycene may effectively prevent the penetration of I^-/I_3^- electrolyte to reach the TiO_2 surface, thereby reducing

* Corresponding authors.
E-mail addresses: zhuyizhou@nankai.edu.cn (Y.-Z. Zhu), jyzheng@nankai.edu.cn (J.-Y. Zheng).

https://doi.org/10.1016/j.jphotochem.2021.113325
Received 2 March 2021; Received in revised form 7 April 2021; Accepted 25 April 2021
Available online 29 April 2021

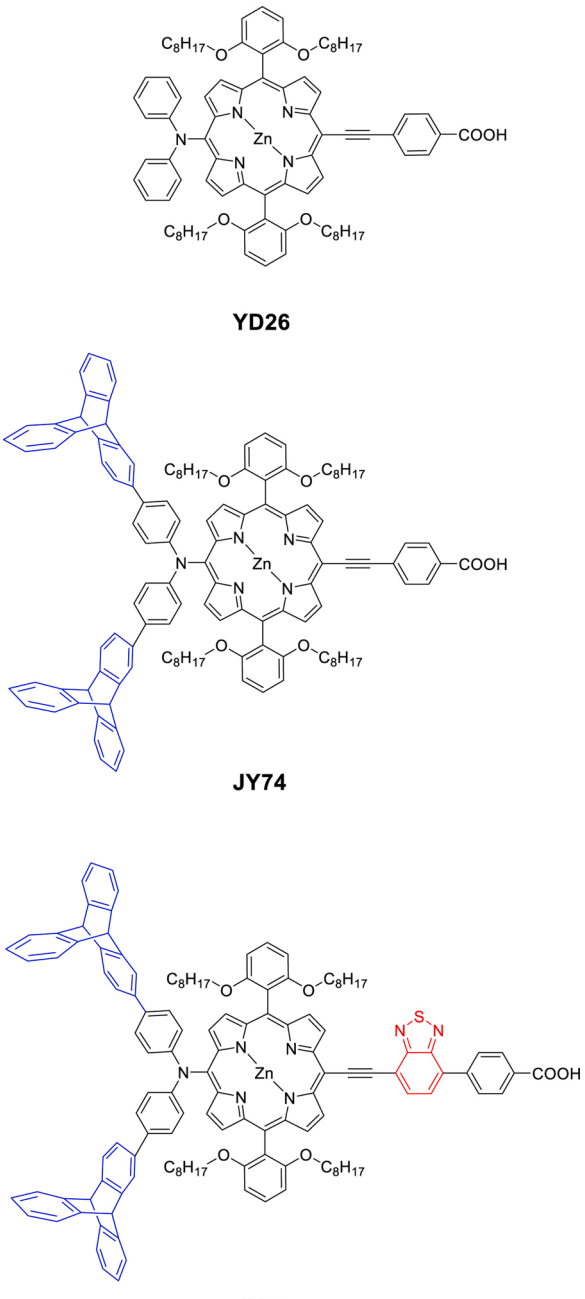

Fig. 1. Chemical structures of dyes **JY74**, **JY75** and reference **YD26**.

the charge recombination and achieving high efficiency. Considering that the superior photovoltaic performance of porphyrin dye in DSSC [22–24], triptycene units were introduced into the terminal diphenylamine of porphyrin-based dye (**YD26**) to form **JY74**. To enhance the light-harvesting capability, auxiliary electron-withdrawing unit 2,1,3-benzothiadiazole (BTD) was further inserted into the backbone of dye **JY74** to give sensitizer **JY75** (Fig. 1) [25]. Optical, electrochemical properties, photovoltaic performance and electrochemical impedance, have been conducted to systematically investigate the substituent effect of triptycene on the porphyrin-embedded skeleton.

2. Experimental

2.1. Materials and instruments

Solvents such as dichloromethane (DCM), petroleum ether (PE), ethyl acetate (EA), 1,4-dioxane, methanol (MeOH), toluene, diethylene glycol dimethyl ether (Diglyme) and acetonitrile (ACN) were used as received, except tetrahydrofuran (THF) was dried over and distilled from sodium/benzophenone under nitrogen.

The ^{1}H NMR and ^{13}C NMR spectra were tested on Bruker 400 MHz spectrometer. HR-MS data were obtained by Varian 7.0 T FT-MS. The absorption spectra of dyes were measured on a Varian Cary 300 Conc. spectrophotometer. Cyclic voltammetry (CV) and electrochemical impedance spectroscopy (EIS) experiments were performed on a Zennium electrochemical workstation (ZAHNER, Germany). Fourier transform infrared (FTIR) spectra were recorded by Nicolet iS50.

2.2. Syntheses of the dyes

The synthetic routes for porphyrin dyes **JY74** and **JY75** are depicted in Scheme 1. 2-Amino-5-bromobenzoic acid reacted with anthracene through Diels-Alder reaction to give intermediate 2-bromotriptycene **3**. Another intermediate **6** was obtained by NBS bromination of diphenylamine and a subsequent Suzuki-coupling with bis(pinacolato) diboron. With them in hand, Buchwald reaction was then performed to yield triptycene-decorated diphenylamine **7** [26]. A hypervalent iodine/Au(III) catalyzed reaction was used to couple the diphenylamine donor **7** and porphyrin precursor **8** [27]. The directly oxidative C–H amination reaction simplifies the synthetic steps and improves the yield in comparison to the synthesis of $\mathbf{D_{26}}$ [12]. When the TIPS group was de-protected by TBAF, palladium promoted Sonogashira reactions were carried out with compounds **10** and **11** respectively to build the dye molecules **JY74** and **JY75**. For the latter, an additional hydrolysis procedure was needed. The synthesis of reference **YD26** refers to the reported literature [12]. All the key intermediates and target dyes were fully characterized with FTIR, NMR and HR-MS.

2.2.1. Synthesis of compound 7

2-Bromotriptycene **3** (700 mg, 2.10 mmol) and compound **6** (354 mg, 0.84 mmol) were mixed in 10 mL of 1:1 (v/v) THF/K_2CO_3 (1 M, aqueous). Then, $Pd_2(dba)_3$ (92.3 mg, 0.10 mmol) and HP(*t*-Bu)$_3$BF$_4$ (73 mg, 0.25 mmol) were added and the reaction mixture heated to reflux for overnight. After cooling to room temperature, the mixture was extracted with DCM (3 × 100 mL), dried over anhydrous $MgSO_4$ and evaporated in vacuum. The residue was purified by column chromatography on silica gel with DCM/PE (1/1) to afford light yellow solid compound **7** (346 mg, 61 %). M.P.: 125−127 °C. ^{1}H NMR (400 MHz, DMSO-d_6) δ 8.41 (s, 1 H), 7.70 (s, 2 H), 7.56−7.37 (m, 14 H), 7.24 (dd, J = 7.7, 1.7 Hz, 2 H), 7.12 (d, J =8.7 Hz, 4 H), 7.10−6.91 (m, 8 H), 5.68 (d, J =11.5 Hz, 4 H). ^{13}C NMR (101 MHz, DMSO-d_6) δ 146.46, 145.73, 145.70, 143.95, 142.90, 137.55, 131.87, 127.83, 125.47, 125.42, 124.43, 124.14, 124.05, 122.81, 121.88, 117.47, 53.24, 52.63. FT-IR (ATR): ν = 3400, 3063, 2954, 2921, 2867, 2850, 1738, 1646, 1603, 1523, 1458, 1401, 1376, 1326, 1285, 1263, 1232, 1188, 1124, 1094, 1082, 1023, 972, 941, 920, 881, 819, 783, 743, 702, 620, 557 and 483 cm^{-1}. HR-MS (MALDI): m/z [M] $^{+}$ calcd for $C_{52}H_{35}N$, 673.2770; found, 673.2766.

2.2.2. Synthesis of compound 9

Compound **8** (164.7 mg, 0.13 mmol), compound **7** (262 mg, 0.39 mmol), PIDA (41.8 mg, 0.13 mmol), and $NaAuCl_4{\cdot}2H_2O$ (77.6 mg, 0.23 mmol) were added to a round-bottom bottle with DCM (15 mL). The reaction mixture was stirred at room temperature for 30 min. Then saturated aqueous solution of $Na_2S_2O_3$ (10 mL) was added. After stirring for another 10 min, the reaction mixture was washed with water three times (3 × 20 mL). The organic layer was filtered through dry silica gel, and evaporated to dryness. The residue was purified by column chromatography using PE/DCM (2/1) to give the compound **9** (170 mg, 70 %). M.P.: 105−108 °C. ^{1}H NMR (400 MHz, chloroform-*d*) δ 9.68 (d, J =4.5 Hz, 2 H), 9.20 (d, J =4.5 Hz, 2 H), 8.88 (d, J =4.5 Hz, 2 H), 8.73 (d, J =4.5 Hz, 2 H), 7.64 (t, J =8.4 Hz, 2 H), 7.51 (s, 2 H), 7.32 (dd, J = 20.7,

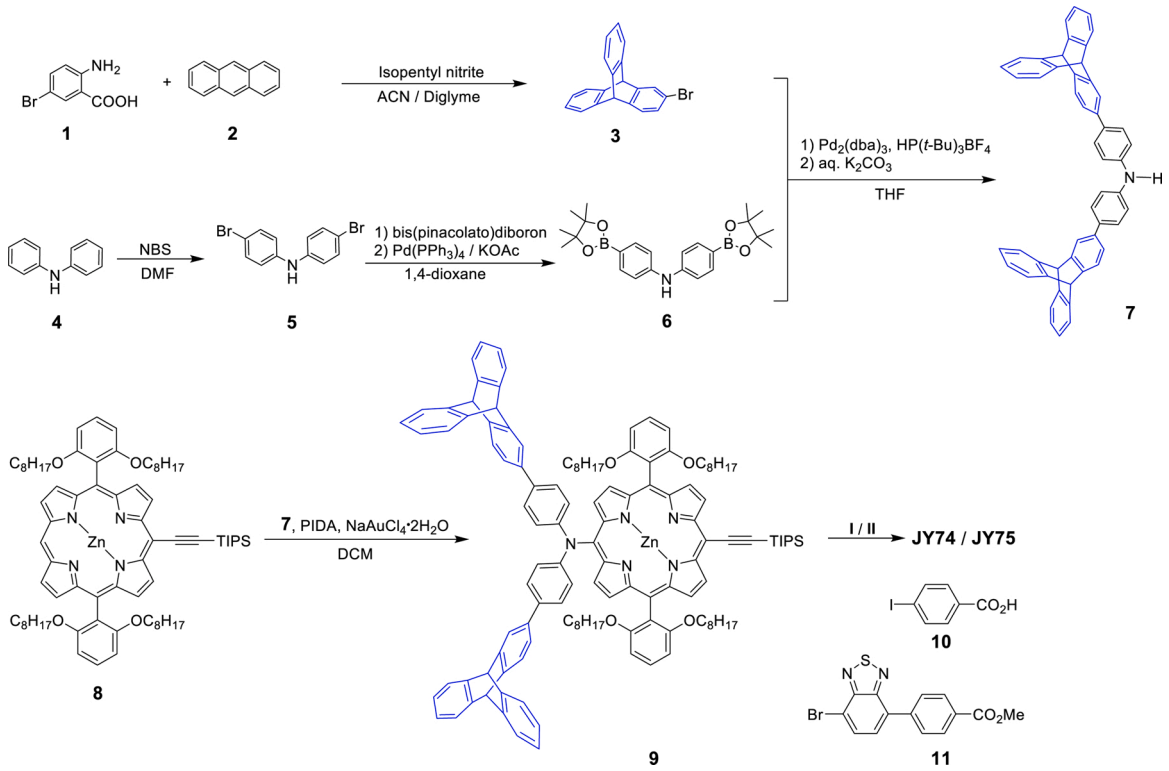

Scheme 1. Synthetic routes of **JY74** and **JY75**. Reaction conditions: (**I**) i: TBAF, THF; ii: **10**, $Pd_2(dba)_3$, $AsPh_3$, Et_3N; (**II**) i: TBAF, THF; ii: **11**, $Pd_2(dba)_3$, $AsPh_3$, Et_3N; iii: 20 % NaOH (aq), THF/MeOH.

6.3 Hz, 18 H), 7.10 (d, J =7.7 Hz, 2 H), 7.01 – 6.92 (m, 12 H), 5.40 (d, J =4.4 Hz, 4 H), 3.82 (t, J =6.3 Hz, 8 H), 1.45 (d, J =4.7 Hz, 18 H), 0.99 (q, J =6.8 Hz, 8 H), 0.92 – 0.84 (m, 3 H), 0.75 (q, J =6.8 Hz, 8 H), 0.61 – 0.35 (m, 44 H). ^{13}C NMR (101 MHz, chloroform-*d*) δ 159.83, 152.51, 151.52, 151.42, 150.68, 150.28, 145.66, 145.22, 143.52, 142.29, 138.13, 132.27, 132.15, 130.75, 130.23, 129.81, 127.56, 125.16, 125.12, 123.73, 123.59, 123.54, 123.38, 122.28, 122.24, 121.92, 120.68, 114.43, 109.94, 105.13, 99.63, 96.40, 68.56, 54.26, 53.66, 31.31, 29.71, 28.51, 28.47, 28.40, 25.08, 22.15, 19.13, 13.74, 11.96. FT-IR (ATR): ν = 3432, 3064, 3019, 2922, 2853, 2134, 1897, 1800, 1589, 1513, 1485, 1456, 1378, 1334, 1321, 1303, 1246, 1211, 1160, 1121, 1188, 1160, 1121, 1098, 1060, 999, 974, 919, 881, 838, 825, 795, 769, 742, 711, 673, 654, 627, 620, 573, 560, 532 and 480 cm^{-1}. HR-MS (MALDI): *m/z* [M] $^+$ calcd for $C_{127}H_{137}N_5O_4SiZn$, 1887.9731; found, 1887.9738.

2.2.3. Synthesis of compound *JY74*

To a stirred solution of compound **9** (90 mg, 0.048 mmol) in THF (10 mL) was added TBAF (0.24 mL, 1 M in THF) under nitrogen. After stirring for 1 h at room temperature, the mixture was diluted with water and extracted with DCM (3 × 100 mL). The organic layer was dried over Na_2SO_4 and concentrated under vacuum. Then the obtained raw material, 4-iodobenzoic acid (47.6 mg, 0.19 mmol), $Pd_2(dba)_3$ (13 mg, 0.014 mmol), and $AsPh_3$ (29 mg, 0.096 mmol) were dissolved in a mixture of THF (20 mL) and Et_3N (5 mL) under nitrogen. The solution was heated at reflux for 6 h. After being cooled down, the reaction mixture was extracted with DCM (3 × 100 mL), the combined organic layer was washed with HCl (1 M aq) and water (100 mL), concentrated in vacuum. The residue was purified by column chromatography using DCM/MeOH (25/1) to give the product **JY74** (76 mg, 85 %). M.P.: 151−154 °C. ^{1}H NMR (400 MHz, chloroform-d) δ 9.69 (d, J =4.4 Hz, 2 H), 9.19 (d, J =4.5 Hz, 2 H), 8.91 (d, J =4.3 Hz, 2 H), 8.72 (d, J =4.4 Hz, 2 H), 8.26 (s, 2 H), 8.10 (d, J =7.5 Hz, 2 H), 7.65 (t, J =8.0 Hz, 2 H), 7.51 (s, 2 H), 7.32 (dd, J = 18.6, 8.3 Hz, 18 H), 7.10 (d, J =7.4 Hz, 2 H), 7.01 – 6.90 (m, 12 H), 5.39 (d, J =3.2 Hz, 4 H), 3.83 (s, 8 H), 1.06 – 0.93 (m, 8 H), 0.77 (dt, J = 13.0, 6.2 Hz, 8 H), 0.66 – 0.40 (m, 44 H). ^{13}C NMR (101 MHz, chloroform-*d*) δ 178.77, 159.83, 152.08, 151.62, 151.43, 150.70, 150.48, 145.70, 145.23, 143.57, 142.71, 141.48, 139.03, 138.10, 135.82, 133.40, 132.38, 131.35, 130.42, 130.31, 129.92, 128.24, 127.58, 125.17, 125.12, 123.73, 123.58, 123.54, 123.38, 122.30, 122.23, 120.55, 114.85, 110.07, 106.97, 105.13, 98.26, 68.54, 54.28, 53.72, 31.36, 29.73, 28.59, 28.55, 28.43, 25.12, 22.23, 13.79. FT-IR (ATR): ν = 3432, 3063, 3019, 2952, 2851, 2186, 1797, 1723, 1688, 1601, 1513, 1485, 1456, 1406, 1377, 1337, 1305, 1288, 1259, 1206, 1172, 1160, 1097, 1061, 997, 973, 920, 881, 856, 823, 794, 769, 741, 712, 671, 664, 627, 620, 559, 503 and 480 cm^{-1}. HR-MS (MALDI): *m/z* [M] $^+$ calcd for $C_{125}H_{121}N_5O_6Zn$, 1851.8608; found, 1851.8613.

2.2.4. Synthesis of compound *JY75*

The ester precursor of **JY75** was prepared in 90 % yield using the same method of **JY74**. Subsequently, 5 mL 20 % NaOH (aq.) was added to the solution of ester precursors of **JY75** (70 mg, 0.035 mmol) in THF (10 mL) and MeOH (8 mL), and stirred at room temperature for overnight. The mixture was extracted with DCM (3 × 100 mL), washed with HCl (1 M aq.) and water (100 mL). The organic layer was dried over anhydrous $MgSO_4$ and concentrated under vacuum, and the residue was purified by column chromatography using DCM/MeOH (20/1) to give the product **JY75** (62 mg, 85 %). M.P.: 147−150 °C. ^{1}H NMR (400 MHz, chloroform-*d*) δ 10.03 (d, J =4.6 Hz, 2 H), 9.18 (d, J =4.6 Hz, 2 H), 8.97 (d, J =4.6 Hz, 2 H), 8.72 (d, J =4.6 Hz, 2 H), 8.31−8.24 (m, 3 H), 8.21 (d, J =8.3 Hz, 2 H), 7.97 (d, J =7.3 Hz, 1 H), 7.66 (t, J =8.4 Hz, 2 H), 7.50 (s, 2 H), 7.41−7.26 (m, 18 H), 7.09 (d, J =6.4 Hz, 2 H), 7.02−6.89 (m, 12 H), 5.38 (d, J =4.5 Hz, 4 H), 3.84 (d, J =2.6 Hz, 8 H), 1.00 (dt, J =6.6 Hz, 8 H), 0.74 (dt, J = 14.5, 6.1 Hz, 8 H), 0.64−0.37 (m, 44 H). ^{13}C NMR (101 MHz, chloroform-*d*) δ 170.75, 159.86, 156.17, 156.14, 153.25, 153.23, 152.47, 152.44, 151.53, 151.44, 150.76, 150.52, 145.70, 145.23, 145.20, 143.58, 143.55, 142.47, 138.08, 133.40,

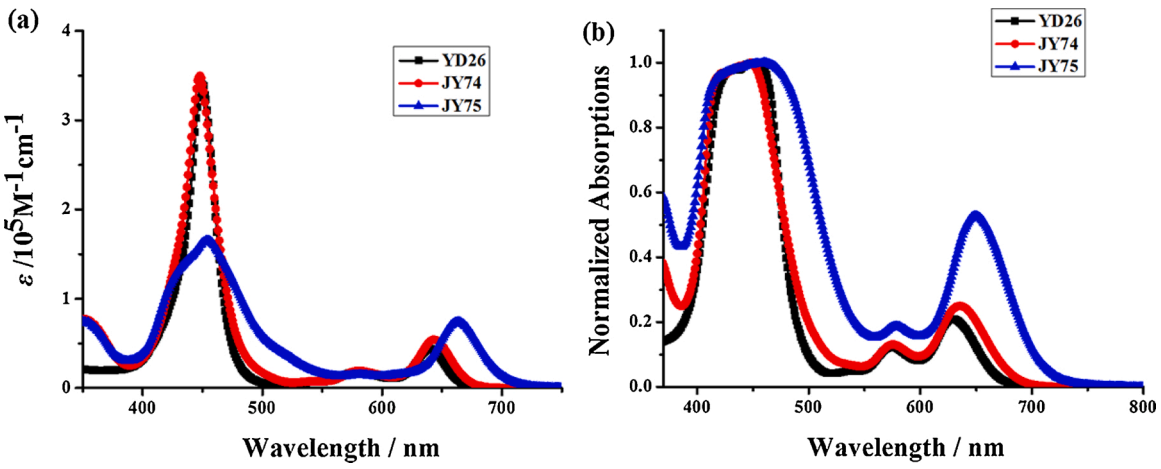

Fig. 2. Absorption spectra of dyes **YD26**, **JY74** and **JY75** (a) in THF solutions and (b) on TiO_2 films (3 μm thickness).

Table 1
Optical and electrochemical properties of the porphyrin-based dyes in THF at 25 °C.

Dyes	Absorption [a] $\lambda_{max/nm}$ ($\varepsilon/10^3$ M^{-1} cm^{-1})	HOMO/V [b] (*vs.* NHE)	E_{0-0}/ eV [c]	LUMO/V [d] (*vs.* NHE)
YD26	448 (339), 580 (17), 639 (44)	0.94	1.86	−0.92
JY74	449 (347), 580 (19), 643 (54)	0.96	1.84	−0.88
JY75	453 (166), 581 (15), 663 (74)	0.91	1.76	−0.85

[a] $\lambda_{max/nm}$ and ε in THF.
[b] The first oxidation potential (HOMO) level was measured in acetonitrile using $TBAPF_6$ as an supporting electrolyte with reference redox couple (Fc/Fc^+), and calibrated.
[c] $E_{0-0} = 1240/\lambda_{onset}$.
[d] The LUMO energy level is estimated by subtracting E_{0-0} from the HOMO energy level.

132.59, 132.29, 131.08, 130.81, 130.51, 129.91, 129.32, 128.70, 127.58, 125.13, 123.70, 123.55, 123.38, 122.64, 122.29, 122.24, 120.64, 118.68, 114.99, 105.16, 101.94, 98.35, 92.07, 68.58, 54.29, 53.70, 31.37, 29.72, 28.56, 28.44, 28.42, 25.09, 22.18, 13.75. FT-IR (ATR): ν = 3432, 3062, 3019, 2950, 2851, 2181, 1717, 1688, 1636, 1590, 1540, 1512, 1485, 1456, 1377, 1337, 1350, 1303, 1287, 1244, 1206, 1184, 1160, 1097, 1019, 996, 972, 942, 928, 833, 823, 794, 770, 742, 712, 670, 652, 627, 620, 558, 535, 503 and 479 cm^{-1}. HR-MS (MALDI): *m/z* [M] $^+$ calcd for $C_{131}H_{123}N_7O_6Zn$, 1985.8547; found, 1985.8551.

3. Results and discussion

3.1. Optical properties

The UV–vis absorption spectra of **YD26**, **JY74** and **JY75** in THF solution and on TiO_2 film are shown in Fig. 2, and the corresponding spectroscopic data are collected in Table 1. The high-energy absorption beneath 400 nm should initiate from to π–π* electronic transitions, and the low-energy region (400–700 nm) stems from the intramolecular charge transfer (ICT) transitions [28,29]. Compared with the reference dye **YD26**, dye **JY74** with triptycene cap presents a negligible change of Soret absorption, but exhibits a slight bathochromic shift in Q-band, suggesting a facilitated ICT process led by triptycene. Owing to the insertion of strong electron-withdrawing BTD, the Soret absorption of **JY75** is split into two peaks, and the maximum absorption of Q-band red-shifts by 20 nm compared to that of **JY74**. Meanwhile, the Q-band molar absorption coefficient of **JY75** (7.4×10^4 M^{-1} cm^{-1}) is calculated to be around 1.3 times than that of **JY74** (5.4×10^4 M^{-1} cm^{-1}). This can be interpreted by the π-extension and symmetry loss caused by the insertion of auxiliary acceptor BTD [30,31]. In addition, the Q-bands of **JY75** are broader than those for **JY74** and **YD26**, revealing that the auxiliary BTD acceptor is effective for enhancing the intramolecular

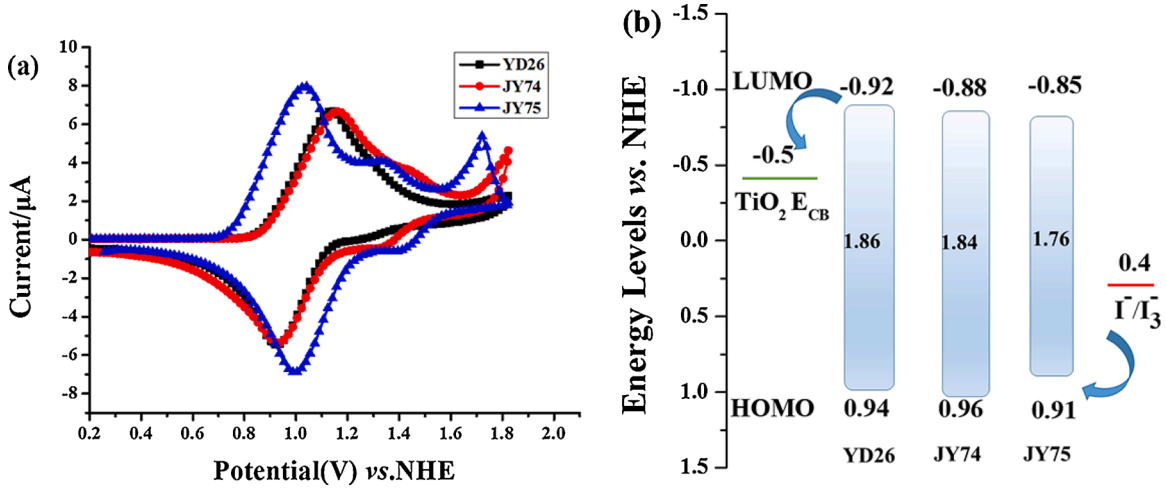

Fig. 3. (a) Cyclic voltammetry curves and (b) schematic energy-level diagrams of the dyes **YD26**, **JY74** and **JY75**.

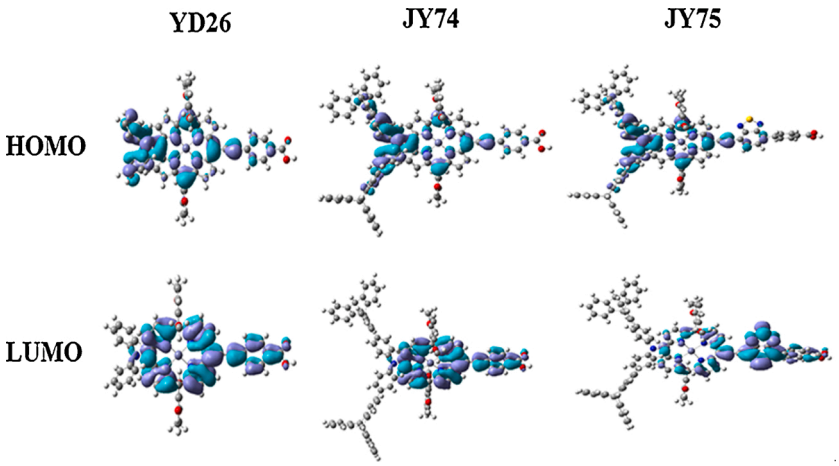

Fig. 4. Frontier molecular orbital diagrams of **YD26**, **JY74** and **JY75**.

charge transfer and extending the absorption. For better understanding of the light-harvesting performance, the absorption properties on the surface of the 3 μm thick TiO_2 films are also studied (Fig. 2b), the absorption ranges of dyes **YD26**, **JY74** and **JY75** are broadened compared to the corresponding absorption spectra in solution, which is favorable for harvesting solar light and achieving high J_{SC}.

3.2. Electrochemical properties

Cyclic voltammetry (CV) was performed to evaluate electron transfer between the excited dyes and the conduction band of TiO_2, as well as the regeneration of the oxidized dyes. As shown in Fig. 3a, using internal reference Fc/Fc^+, the ground-state oxidation potentials (E_{OX}) of **YD26**, **JY74** and **JY75** are estimated to be 0.94, 0.96 and 0.91 V, respectively (*vs.* NHE, Table 1). The more positive E_{OX} values relative to I^-/I_3^- redox shuttle (~ 0.4 V), affording a smooth regeneration of the oxidized dyes under the electrolyte. The excited-state oxidation potentials (E_{OX}^*) of **YD26**, **JY74** and **JY75** are calculated from the equation of $E_{OX}^* = E_{OX} - E_{0-0}$, to be – 0.92, – 0.88 and – 0.85 V, respectively, which are obviously negative than the TiO_2 conduction band (~ – 0.5 V) and guarantee a fast electron injection dynamics [32]. Since E_{OX} and E_{OX}^*, respectively, correspond to the HOMO and LUMO energies, a schematic diagram about the energy-levels of **YD26**, **JY74** and **JY75** can be built (Fig. 3b). Apparently, the introduction of BTD makes dye **JY75** a relatively narrow HOMO-LUMO energy gap in comparison to that of **YD26** and **JY74**, in good accordance with its much red-shifted absorption. Under the premise of ensuring sufficient injection driving force, the reduction of LUMO level in dye **JY75** is beneficial for diminishing the energy loss of excited state [33]. It further explains the reason why the open-circuit voltage of **JY75** increases.

3.3. Theoretical studies

To get qualitative in-depth information on the optimized configurations and frontier molecular orbitals of **YD26**, **JY74** and **JY75** sensitizers, density functional theory (DFT) calculations were performed with a functional basis set of B3LYP/6−31 G(d,p) level [34]. Fig. 4 exhibits the optimized ground-state structures of dyes **YD26**, **JY74** and **JY75**. The HOMO levels of **YD26**, **JY74** and **JY75** delocalize throughout the diphenylamine donor and porphyrin ring, and the LUMO orbitals diffuse mainly on porphyrin ring and the acceptor, a good overlap occurs on porphyrin moiety. Notably, dye **JY75** shows lower electron-density distribution of LUMO orbitals on the porphyrin framework in comparison to dyes **YD26** and **JY74** because of the involved auxiliary electron-withdrawing BTD. Such orbital distribution of these dyes is conducive to the electron transfer from HOMO to LUMO, and subsequent photo-induced charge injection from the LUMO to the conduction band of TiO_2.

Experiments of time-resolved luminescence in THF and on TiO_2 surface were performed to better understand the electron injection dynamics of the dyes (Fig. S14) [22,23]. The fluorescence lifetimes of **YD26**, **JY74** and **JY75** in THF were measured to be 2.35, 2.69 and 1.67 ns, respectively. When fixed on the surface of TiO_2, the emissions of dyes **YD26**, **JY74** and **JY75** were strongly quenched, and the related

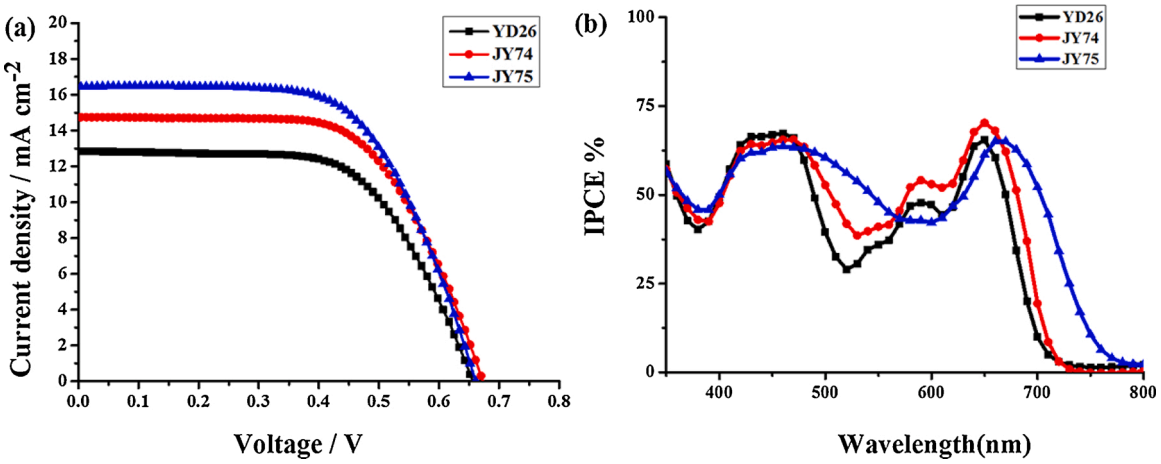

Fig. 5. (a) *J–V* curves and (b) IPCE action spectra of the DSSCs based on **YD26**, **JY74** and **JY 75**.

Table 2
Photovoltaic performance of devices [a].

Dye	V_{OC}/mV	J_{SC}/mA cm^{-2}	*FF*	η/%
YD26	662 ± 3	12.92 ± 0.16	0.62 ± 0.01	5.34 ± 0.04
JY74	681 ± 4	14.58 ± 0.39	0.63 ± 0.00	6.29 ± 0.17
JY75	673 ± 5	16.50 ± 0.22	0.61 ± 0.01	6.77 ± 0.04

[a] The active area of the cell was 0.196 cm^2.

lifetimes decline to 144, 79 and 68 ps, respectively. The significant decrease of fluorescence decay lifetime may suggest a highly efficient electron injection.

3.4. Photovoltaic performance

Devices based on dyes **YD26**, **JY74** and **JY75** were fabricated with iodine electrolyte, and were measured under AM 1.5 G irradiation. The photocurrent density − voltage (J−V) curves and incident photon-to-current conversion efficiency (IPCE) spectra are shown in Fig. 5, and the details of photovoltaic parameters are collected in Table 2. All the IPCE spectra give a broad absorption range ending over 700 nm (Fig. 5b), indicating an efficient photo-to-current conversion. Compared with **YD26**, dyes **JY74** and **JY75** featuring triptycene modified diphenylamine show much higher J_{SC} values, meantime the J_{SC} order is in good accordance with their IPCE tendency. Notable increase of J_{SC} has been observed for **JY75** owing to its large π-extension and enhanced ICT caused by the presence of BTD unit. As for V_{OC}, dye **JY74** shows higher value relative to that of **YD26**, revealing that the presence of triptycene may ameliorate the charge recombination. That is further confirmed by the somewhat higher V_{OC} of dye **JY75** against that of **YD26**, considering that the auxiliary acceptor BTD often leads to a significant V_{OC} drop due to its strong electron-trap effect. As a result, both **JY74** and **JY75** give a higher PCE than that of **YD26**, and dye **JY75** achieves the highest efficiency of 6.77 %. Hence, the synchronous introduction of a donor featuring triptycene-like bulky rigid steric hindrance group and a BTD-like acceptor can synergistically enhance V_{OC} and J_{SC} values, resulting in improved photovoltaic efficiencies.

3.5. Electrochemical impedance spectroscopy

Electrochemical impedance spectroscopies (EIS) of **YD26**, **JY74** and **JY75** based-devices were measured in darkness to get a comprehensive exploration of the charge transfer process at interface [35,36]. Nyquist and Bode diagrams were obtained under a − 0.64 V bias within a frequency ranging from 100 kHz to 0.1 Hz and curved in Fig. 6. The interfacial charge transfer resistance (R_{CT}) at the interfaces of TiO_2/-dye/electrolyte can be obtained by the larger semicircle in the Nyquist diagram. The R_{CT} values increases in the order of **YD26** (99.1 Ω) < **JY75** (115.6 Ω) < **JY74** (133.9 Ω), which falls in accordance with the V_{OC} tendency of **YD26** (662 mV) < **JY75** (673 mV) < **JY74** (681 mV), demonstrating an inferior charge recombination of **JY74**. Electron lifetime (τ) can be evaluated by $\tau = 1/(2\pi f)$ and where f represents the peak frequency. Accordingly, the relative τ values of **YD26**, **JY74**, and **JY75** should be 14.03, 25.64 and 15.02 ms. The relatively larger τ relates to a smaller dark current, which further explains the superior V_{OC} of **JY74**.

In order to further explore the role of triptycene in shielding off I^-/I_3^- electrolytes, electrostatic potentials (VE) of three dyes have been obtained after optimizing in their neutral form [37]. In Fig. S15, the blue-colored surfaces indicate the positively charged regions, which are more favorable points for interacting with iodide. In comparison to the computed electrostatic potentials map of **YD26**, dyes **JY74** and **JY75** show obviously positive charge distribution on triptycene. Consequently, I^-/I_3^- electrolyte in **JY74** and **JY75** based devices will be more localized near triptycene-modified donors through electrostatic interaction, thus reducing the contact between I^-/I_3^- electrolyte and TiO_2 and inhibiting electron recombination. Finally, it leads to the improvement of photovoltaic performance.

4. Conclusions

In conclusion, the triptycene unit with three-dimensional rigidity was rationally introduced into porphyrin dyes (**JY74** and **JY75)** and applied to fabricate DSSCs for the first time. The influence of bulky rigid steric hindrance group triptycene and electron-withdrawing unit of BTD on the photophysical properties and photovoltaic performance was investigated. As expected, dye **JY74** with triptycene cap exhibits not only broadened absorption but also reduced charge recombination, presenting obvious improvement in J_{SC} and V_{OC}. Auxiliary BTD unit further increases the J_{SC} of **JY75**, and guarantees the highest PCE of 6.77 %.

CRediT authorship contribution statement

Mao Yan: Conceptualization, Investigation, Writing - original draft. **Qun-Hui Wang:** Investigation, Data curation. **Yi-Zhou Zhu:** Supervision, Writing - review & editing. **Ming-Liang Han:** Investigation. **Yi-Qiao Yan:** Validation. **Jian-Yu Zheng:** Supervision, Funding acquisition, Writing - review & editing.

Declaration of Competing Interest

The authors report no declarations of interest.

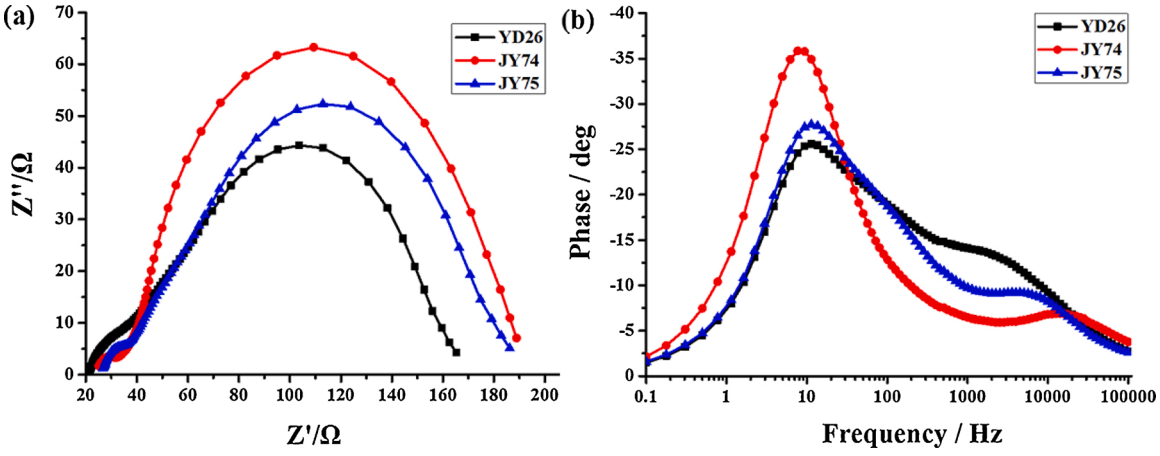

Fig. 6. (a) The Nyquist plots and (b) the Bode phase plots of DSSCs based on dyes **YD26**, **JY74** and **JY75** in dark.

Acknowledgement

We are grateful to the National Natural Science Foundation of China (Nos. 21572108, 21971128 and 21935007) for their generous financial support.

Appendix A. Supplementary data

Supplementary material related to this article can be found, in the online version, at doi:https://doi.org/10.1016/j.jphotochem.2021.113325.

References

[1] M. Urbani, M. Grätzel, M.K. Nazeeruddin, T. Torres, Meso-substituted porphyrins for dye-sensitized solar cells, Chem. Rev. 114 (2014) 12330–12396, https://doi.org/10.1021/cr5001964.
[2] F.F. Gao, Y. Wang, D. Shi, J. Zhang, M.K. Wang, X.Y. Jing, R. Humphry-Baker, P. Wang, S.M. Zakeeruddin, M. Grätzel, Enhance the optical absorptivity of nanocrystalline TiO_2 film with high molar extinction coefficient ruthenium sensitizers for high performance dye-sensitized solar cells, J. Am. Chem. Soc. 130 (2008) 10720–10728, https://doi.org/10.1021/ja801942j.
[3] L. Zhao, P. Wagner, H.V. Salm, T.M. Clarke, K.C. Gordon, S. Mori, A.J. Mozer, Dichromophoric zinc porphyrins: filling the absorption gap between the Soret and Q bands, J. Phys. Chem. C. 119 (2015) 5350–5363, https://doi.org/10.1021/acs.jpcc.5b00147.
[4] T. Higashino, K. Kawamoto, K. Sugiura, Y. Fujimori, Y. Tsuji, K. Kurotobi, S. Ito, H. Imahori, Effects of bulky substituents of push-pull porphyrins on photovoltaic properties of dye-sensitized solar cells, ACS Appl. Mater. Interfaces 8 (2016) 15379–15390, https://doi.org/10.1021/acsami.6b03806.
[5] Y. Kurumisawa, T. Higashino, S. Nimura, Y. Tsuji, H. Iiyama, H. Imahori, Renaissance of fused porphyrins: substituted methylene-bridged thiophene-fused strategy for high-performance dye-sensitized solar cells, J. Am. Chem. Soc. 141 (2019) 9910–9919, https://doi.org/10.1021/jacs.9b03302.
[6] S.H. Kang, M.J. Jeong, S.M. Kwon, I.T. Choi, S.M. Kwon, Y.J. Yoo, J. Kim, J. Kwon, J.H. Park, H.K. Kim, Porphyrin sensitizers with donor structural engineering for superior performance dye-sensitized solar cells and tandem solar cells for water splitting applications, Adv. Energy Mater. 7 (2017) 1602117, https://doi.org/10.1002/aenm.201602117.
[7] M.-L. Han, Y.-Z. Zhu, S. Liu, Q.-L. Liu, D. Ye, B. Wang, J.-Y. Zheng, The improved photovoltaic performance of phenothiazine-dithienopyrrole based dyes with auxiliary acceptors, J. Power Sources 387 (2018) 117–125, https://doi.org/10.1016/j.jpowsour.2018.03.059.
[8] Z.Y. Yao, M. Zhang, L. Yang, R.Z. Li, P. Wang, Donor/acceptor indenoperylene dye for highly efficient organic dye-sensitized solar cells, J. Am. Chem. Soc. 137 (2015) 3799–3802, https://doi.org/10.1021/jacs.5b01537.
[9] Z.Y. Yao, M. Zhang, R.Z. Li, L. Yang, Y.N. Qiao, P. Wang, A metal-free *N*-annulated thienocyclopentaperylene dye: power conversion efficiency of 12% for dye-sensitized solar cells, Angew. Chem. Int. Ed. 54 (2015) 5994–5998, https://doi.org/10.1002/anie.201501195.
[10] H. Imahori, T. Umeyama, S. Ito, Large π-aromatic molecules as potential sensitizers for highly efficient dye-sensitized solar cells, Acc. Chem. Res. 42 (2009) 1809–1818, https://doi.org/10.1021/ar900034t.
[11] Z.S. Wang, N. Koumura, Y. Cui, M. Takahashi, H. Sekiguchi, A. Mori, T. Kubo, A. Furube, K. Hara, Hexylthiophene-functionalized carbazole dyes for efficient molecular photovoltaics: tuning of solar-cell performance by structural modification, Chem. Mater. 20 (2008) 3993–4003, https://doi.org/10.1021/cm8003276.
[12] H.H. Chou, K.S. Reddy, H.P. Wu, B.C. Guo, H.W. Lee, E.W.G. Diau, C.P. Hsu, C. Y. Yeh, Influence of phenylethynylene of push-pull zinc porphyrins on the photovoltaic performance, ACS Appl. Mater. Interfaces 8 (2016) 3418–3427, https://doi.org/10.1021/acsami.5b11554.
[13] E. Mosconi, J.H. Yum, F. Kessler, G. Gomez, J. Carlos, Cobalt electrolyte/dye interactions in dye-sensitized solar cells: a combined computational and experimental study, J. Am. Chem. Soc. 134 (2012) 19438–19453, https://doi.org/10.1021/ja3079016.
[14] P. Gao, Y.J. Kim, J.H. Yum, T.W. Holcombe, M.K. Nazeeruddin, M. Grätzel, Facile synthesis of a bulky BPTPA donor group suitable for cobalt electrolyte based dye sensitized solar cells, J. Mater. Chem. A 1 (2013) 5535–5544, https://doi.org/10.1039/C3TA10632B.
[15] H.L. Jia, M.D. Zhang, W. Yan, X.H. Jun, H. Zheng, Effects of structural optimization on the performance of dye-sensitized solar cells: spirobifluorene as a promising building block to enhance V_{oc}, J. Mater. Chem. A 4 (2016) 11782–11788, https://doi.org/10.1039/C6TA03740B.
[16] S. Chang, H.D. Wang, Y. Hua, Q. Li, X.D. Xiao, W.K. Wong, W.Y. Wong, X.J. Zhu, T. Chen, Conformational engineering of co-sensitizers to retard back charge transfer for high-efficiency dye-sensitized solar cells, J. Mater. Chem. A 1 (2013) 11553–11558, https://doi.org/10.1039/C3TA12714A.
[17] P.D. Bartlett, M.J. Ryan, S.G. Cohen, Triptycene (9,10-*o*-Benzenoanthracene), J. Am. Chem. Soc. 64 (1942) 2649–2653, https://doi.org/10.1021/ja01263a035.
[18] T. Kobayashi, T. Kubota, K. Ezumi, Intramolecular orbital interactions in triptycene studied by photoelectron spectroscopy, J. Am. Chem. Soc. 105 (1983) 2172–2174, https://doi.org/10.1021/ja00346a012.
[19] E.H. Menke, V. Lami, M. Mastalerz, Y. Vaynzof, π-Extended rigid triptycene-trisaroylenimidazoles as electron acceptors, Chem. Commun. 52 (2016) 1048–1051, https://doi.org/10.1039/C5CC07238G.
[20] E.H. Menke, D. Leibold, V. Lami, Y.J. Hofstetter, M. Mastalerz, Y. Vaynzof, Triptycene-trisaroyleneimidazoles as non-fullerene acceptors-influence of side-chains on solubility, device morphology and performance, Org. Electron. 47 (2017) 211–219, https://doi.org/10.1016/j.orgel.2017.05.004.
[21] Y. Zhang, B. Kan, X. Ke, Y.C. Wang, H.R. Feng, H.T. Zhang, C.X. Li, X.J. Wan, Y. S. Chen, 3-Dimensional non-fullerene acceptors based on triptycene and perylene diimide for organic solar cells, Org. Electron. 50 (2017) 458–465, https://doi.org/10.1016/j.orgel.2017.07.021.
[22] A. Yella, H.W. Lee, H.N. Tsao, C.Y. Nazeeruddin, E.W.G. Diau, C.Y. Yeh, S. M. Zakeeruddin, M. Grätzel, Porphyrin-sensitized solar cells with cobalt (II/III)–based redox electrolyte exceed 12 percent efficiency, Science 334 (2011) 629–634, https://doi.org/10.1126/science.1209688.
[23] S. Mathew, A. Yella, P. Gao, H.B. Robin, N.A. Astani, I. Tavernelli, U. Rothlisberger, M.K. Nazeeruddin, M. Grätzel, Dye-sensitized solar cells with 13% efficiency achieved through the molecular engineering of porphyrin sensitizers, Nat. Chem. 6 (2014) 242–247, https://doi.org/10.1038/nchem.1861.
[24] J.F. Lu, H. Li, S.S. Liu, Y.C. Chang, H.P. Wu, Y.B. Cheng, E.W.G. Diau, M.K. Wang, Novel porphyrin-preparation, characterization, and applications in solar energy conversion, Phys. Chem. Chem. Phys. 18 (2016) 6885–6892, https://doi.org/10.1039/C5CP05658F.
[25] K.V.S. Krishna, D. Koteshwar, T.H. Chowdhury, S.P. Singh, I. Bedja, A. Islam, L. Giribabu, Efficient near IR porphyrins containing a triphenylamine-substituted anthryl donating group for dye sensitized solar cells, J. Mater. Chem. C 7 (2019) 13594–13605, https://doi.org/10.1039/C9TC03943K.
[26] D. Reinhard, F. Rominger, M. Mastalerz, Synthesis of triphenylene-based triptycenes via Suzuki-Miyaura cross-coupling and subsequent Scholl reaction, J. Org. Chem. 80 (2015) 9342–9348, https://doi.org/10.1021/acs.joc.5b01520.
[27] D.M. Shen, C. Liu, X.G. Chen, Q.Y. Chen, Facile and efficient hypervalent iodine (III)-mediated *meso*-functionalization of porphyrins, J. Org. Chem. 74 (2009) 206–211, https://doi.org/10.1021/jo801855d.
[28] W.X. Gao, M. Liang, Y.L. Tan, M. Wang, Z. Sun, S. Xue, New triarylamine sensitizers for high efficiency dye-sensitized solar cells: recombination kinetics of cobalt(III) complexes at titania/dye interface, J. Power Sources 283 (2015) 260–269, https://doi.org/10.1016/j.jpowsour.2015.02.121.
[29] Q.Y. Feng, Q. Zhang, X.F. Lu, H. Wang, G. Zhou, Z.S. Wang, Facile and selective synthesis of oligothiophene-based sensitizer isomers: an approach toward efficient dye-sensitized solar cells, ACS Appl. Mater. Interfaces 5 (2013) 8982–8990, https://doi.org/10.1021/am402036j.
[30] P.-P. Dai, Y.-Z. Zhu, Q.-L. Liu, Y.-Q. Yan, J.-Y. Zheng, Novel indeno[1,2-*b*]indole-spirofluorene donor block for efficient sensitizers in dye-sensitized solar cells, Dyes Pigm. 175 (2020) 108099–108106, https://doi.org/10.1016/j.dyepig.2019.108099.
[31] B. Pan, Y.-Z. Zhu, D. Ye, J.-Y. Zheng, Improved conversion efficiency in dye-sensitized solar cells: based on porphyrin dyes with dithieno[3,2-b:2′,3′-d]pyrrole donor, Dyes Pigm. 150 (2018) 223–230, https://doi.org/10.1016/j.dyepig.2017.12.018.
[32] H.R. Zhou, J.M. Ji, S.H. Kang, M.S. Kim, H.S. Lee, C.H. Kim, H.K. Kim, Molecular design and synthesis of D-π-A structured porphyrin dyes with various acceptor units for dye-sensitized solar cells, J. Mater. Chem. C 7 (2019) 2843–2852, https://doi.org/10.1039/C8TC05283B.
[33] L. Zhang, X.C. Yang, W.H. Wang, G.H. Gurzadyan, J.J. Li, X.X. Li, J.C. An, Z. Yu, H. X. Wang, B. Cai, A. Hagfeldt, L.H. Sun, 13.6% efficient organic dye-sensitized solar cells by minimizing energy losses of the excited state, ACS Energy Lett. 4 (2019) 943–951, https://doi.org/10.1021/acsenergylett.9b00141.
[34] A.D. Becke, Density-functional thermochemistry. III. The role of exact exchange, J. Chem. Phys. 98 (1993) 5648–5652, https://doi.org/10.1063/1.464913.
[35] Y.D. Lin, B.Y. Ke, Y.J. Chang, P.T. Chou, K.L. Liau, C.Y. Liu, T.J. Chow, Pyridomethene-BF_2 complex/phenothiazine hybrid sensitizer with high molar extinction coefficient for efficient, sensitized solar cells, J. Mater. Chem. A 3 (2015) 16831–16842, https://doi.org/10.1039/C5TA03807C.
[36] G.B. Bodedla, K.R. Justin Thomas, M.S. Fan, K.C. Ho, Benzimidazole-Branched isomeric dyes: effect of molecular constitution on photophysical, electrochemical, and photovoltaic properties, J. Org. Chem. 81 (2016) 640–653, https://doi.org/10.1021/acs.joc.5b02590.
[37] C. Aumaitre, R.S. Cristina, J. Jover, O. Bardagot, F. Caffy, Y. Kervella, N. Lopez, E. Palomares, R. Demadrille, Visible and near-infrared organic photosensitizers comprising isoindigo derivatives as chromophores: synthesis, optoelectronic properties and factors limiting their efficiency in dye solar cells, J. Mater. Chem. A 6 (2018) 10074–10084, https://doi.org/10.1039/C8TA01826J.